Research Article

Journal of Environmental Nanotechnology

Green Sol–gel Synthesis of Cu/Co_3O_4 Nanocomposite Using *Curcuma Longa* Leaf Extract for High-performance Supercapacitor Electrodes

H. V. Ganvir[1*], Haitham M. Hadidi[2], Rajasekaran Saminathan[2], Madhuri S. Bhagat[3], C. Krishnaraj[4] and P. Satishkumar[4]

[1]Department of Applied Physics, Yeshwantrao Chavan College of Engineering Nagpur, MH, India
[2]Department of Mechanical Engineering, College of Engineering and Computer Science, Jazan University, Jazan, Kingdom of Saudi Arabia
[3]Department of Civil Engineering, Yeshwantrao Chavan College of Engineering, Nagpur, MH, India
[4]Department of Mechanical Engineering, Rathinam Technical Campus, Coimbatore, TN, India
Received: 25.12.2025 Accepted: 07.02.2026 Published: 30.03.2026
*hrwasnik@gmail.com

ABSTRACT

Cobalt oxide (Co_3O_4)–based nanocomposites have attracted considerable attention as promising electrode materials for high-performance supercapacitors due to their rich redox activity and structural stability. In this work, a Cu/Co_3O_4 nanocomposite was synthesized *via* a green sol–gel route using *Curcuma longa* leaf extract as a natural reducing and stabilizing agent. UV–Vis spectroscopy revealed characteristic absorption bands at 333.1 and 373.3 nm, while XRD and SEM analyses confirmed the formation of crystalline Cu/Co_3O_4 nanorods with uniform morphology. The electrochemical behavior of the fabricated Cu/Co_3O_4 electrode was evaluated in 1 M KOH using cyclic voltammetry, galvanostatic charge–discharge, and electrochemical impedance spectroscopy. The electrode exhibited dominant pseudocapacitive behavior with a high specific capacitance of 345 F g^{-1} at 1 A g^{-1}, excellent cycling stability with 95.3% capacitance retention after 5000 cycles, and a coulombic efficiency of ~99%. The low charge-transfer resistance and favorable ion-diffusion characteristics further confirm the efficient charge-storage kinetics of the nanocomposite. These results demonstrate that the green-synthesized Cu/Co_3O_4 nanocomposite is a viable and sustainable electrode material for advanced electrochemical energy-storage applications.

Keywords: Composite synthesis; Energy storage; Supercapacitor; Electrochemical properties; Nanorods.

1. INTRODUCTION

Supercapacitors are promising energy-storage devices; however, the development of sustainable, low-cost, and high-performance electrode materials remains a major challenge. Unlike lithium-ion batteries and fuel cells, they store energy through fast surface or redox-based mechanisms, enabling instant energy delivery for modern applications (Ganvir *et al*. 2024). With the expansion of renewable energy systems, electric vehicles and smart electronics, demand for supercapacitors has grown rapidly in recent years (Anantha *et al*. 2025). The versatility, reliability, and environmental compatibility make them a key component in next-generation sustainable energy-storage solutions. Rising supercapacitor adoption highlights the potential of nanorods, which exhibit high capacitance and stability for advanced energy-storage devices (Khawale *et al*. 2024). Researchers developed a carbon-fiber supercapacitor using MOF-derived Fe_2O_3 and Co_3O_4 coatings, achieving improved pseudocapacitive storage. The device shows 22.2 mWh/kg energy density and strong mechanical strength for multifunctional EV applications (González-Banciella *et al*. 2026).

Green-synthesized AgNPs from Moringa and Curcuma showed strong antioxidant and antibacterial activity, with conjugated antibiotic–AgNPs performing even better (Din *et al*. 2024; Singh *et al*. 2025). Previous studies confirm that *Curcuma longa* leaf extract acts as an effective natural reducing and stabilizing agent, supporting its suitability for green nanomaterial synthesis (Anekwe *et al*. 2023). Fe- and Cu-doped Co_3O_4 spinels improved capacitance (up to 1350 F/g) with fast redox kinetics. Low internal resistance and stable ion transport make them promising for flexible supercapacitors (Samatha and Sagar, 2025). Although Cu–Co–based oxides and MOF-derived heterostructures have demonstrated high specific capacitance (1100–1600 F g^{-1}), many of these materials rely on complex synthesis routes, high temperatures, or costly precursors, limiting scalability (Mendhe *et al*. 2025; Kumar *et al*. 2025). Cu-

substituted Co_3O_4 (1:4 ratio) enhanced electron transfer and oxygen density, yielding 775 F/g. The hybrid supercapacitor achieved 27.9 Wh/kg with good cycling stability (Zhang *et al*. 2025). Activated PANI-derived carbon with MnO_2 achieved high surface area and 357 F/g capacitance. Its porous structure makes it a strong candidate for efficient and low-cost supercapacitors (Alaş Çolak *et al*. 2025). Zn–Cu co-doped Co_3O_4 spinels with nanowire/nanoribbon flower-like structures showed enhanced ion diffusion and oxygen-vacancy–induced redox activity. The optimized $Zn_{0.5}Cu_{0.5}Co_2O_4$ delivered 1776 F/g and 122.2 Wh/kg, maintaining excellent cycling stability (Yesuraj *et al*. 2025). MOF-derived $CuCo_2O_4$ with coral-reef morphology showed strong OER activity (η = 317 mV, 49 mV dec^{-1}) and high stability. As a supercapacitor electrode, it delivered 75 C/g, outperforming CuO and Co_3O_4 (Da Silva *et al*. 2025). Despite extensive studies on Cu–Co oxide electrodes, reports on plant-mediated sol–gel synthesis of Cu/Co_3O_4 nanocomposites for supercapacitor applications remain limited.

Flower-like $CuCo_2O_4$ microstructures synthesized solvothermally acted as efficient battery-type cathode materials. They achieved 627 C/g capacity with excellent cycling stability, confirming suitability for hybrid supercapacitors (Hari *et al*. 2024). Co_3O_4-incorporated CuHCF composites showed a dramatic capacitance boost to 1456 F/g due to abundant electroactive sites and synergistic redox couples. The material retained 85% performance after 2500 cycles, making it highly promising for flexible supercapacitors (Shuaib *et al*. 2024). Zinc sulfate–supported Co_3O_4 nanoparticles synthesized *via* microwave irradiation showed good crystallinity and metal–oxygen functionality. They exhibited notable antibacterial and antifungal activity, indicating strong biomedical potential (Mayakannan *et al*. 2023a). Copper-doped Co_3O_4 nanoparticles with ~20 nm crystallite size was synthesized, showing needle-like morphology and a 4.52 eV indirect bandgap. Structural and optical analyses confirmed successful doping and nanostructure formation (Mayakannan *et al*. 2023b). Silver-doped Co_3O_4 nanoparticles displayed increasing crystallite size with higher Ag content and showed cubic/spherical morphology. The 20 wt% Ag-doped sample exhibited the best antibacterial activity with reduced bandgap (Gopinath *et al*. 2022).

This technique has several advantages, including user-friendliness, consistency, affordability, and low processing temperature. Accordingly, this study reports a green sol–gel synthesis of a Cu/Co_3O_4 nanocomposite using *Curcuma longa* leaf extract and systematically evaluates its electrochemical performance as a supercapacitor electrode. Additionally, it assesses (i) the factors adding efficacy of the Cu/Co_3O_4 nanocomposite, and (ii) the underlying processes involved. To the best of our knowledge, limited studies have reported green sol–gel synthesized Cu/Co_3O_4 nanocomposites derived from plant extracts for supercapacitor electrode applications.

2. MATERIAL AND METHODS

2.1 Materials

Matrics Enterprises, located in Nagercoil, Tamil Nadu, India, provided 99.9% pure copper nitrate trihydrate and cobalt nitrate hexahydrate. Tartaric acid ($C_4H_6O_6$) was obtained from Star Scientific in Erode, Tamil Nadu, India. Homogeneous *Curcuma longa* leaves were collected from Erode agricultural fields. Double-distilled water (DD) was utilized across the whole procedure.

2.2 Preparation of Cu/Co_3O_4 Nanocomposite

Copper nitrate trihydrate ($Cu(NO_3)_2{\cdot}3H_2O$) was dissolved in double-distilled water to obtain a 0.1 M solution, while cobalt nitrate hexahydrate ($Co(NO_3)_2{\cdot}6H_2O$) was prepared separately at the same molar concentration, maintaining a Cu:Co molar ratio of 1:1. The subsequent phase was the incremental incorporation of *Curcuma longa* leaf extract. A fixed volume of 5 mL of *Curcuma longa* leaf extract (corresponding to 10 vol% of the precursor solution) was added dropwise as a reducing and stabilizing agent. The procedure for extracting *Curcuma longa* leaf extract (Gopan *et al*. 2025). The incorporation at a temperature of 40 °C, with continuous stirring of the solution for 90 minutes, facilitated stabilization of the copper NPs (Cu nanoparticles). The solution's color transformed into a rich brown. About 1 mol of cobalt nitrate hexahydrate ($Co(NO_3)_2{\cdot}6H_2O$) was dissolved in 50 mL of water. Then, 10 mL of leaf extract was incorporated incrementally. The phytochemicals present in *Curcuma longa* leaf extract, such as polyphenols and flavonoids, act as natural reducing agents for metal ions and simultaneously stabilize the formed nanoparticles through surface capping. The color of the solution changed from black to white. The subsequent stage involved mixing the copper and cobalt solutions, followed by the addition of 1 mole of tartaric acid. The mixture was subsequently stirred constantly at 60 °C for 6 hours (Liu *et al*. 2020). An overnight duration in the oven at 120 °C yielded the formation of a gel. The final black powder was calcined in a tube furnace at 400 °C. Subsequent to cleaning with double-distilled water and ethanol, the fine powder was allowed to dry at oven maintained at 60 °C.

Fig. 1 presents a block diagram illustrating the overall methodology adopted in this study, including the green sol–gel synthesis of the Cu/Co_3O_4 nanocomposite using *Curcuma longa* leaf extract, electrode fabrication, and electrochemical characterization. The block diagram provides a clear overview of the interaction between the metal precursors, plant extract, sol–gel precursor formation, nanocomposite development, and its subsequent application as a supercapacitor electrode.

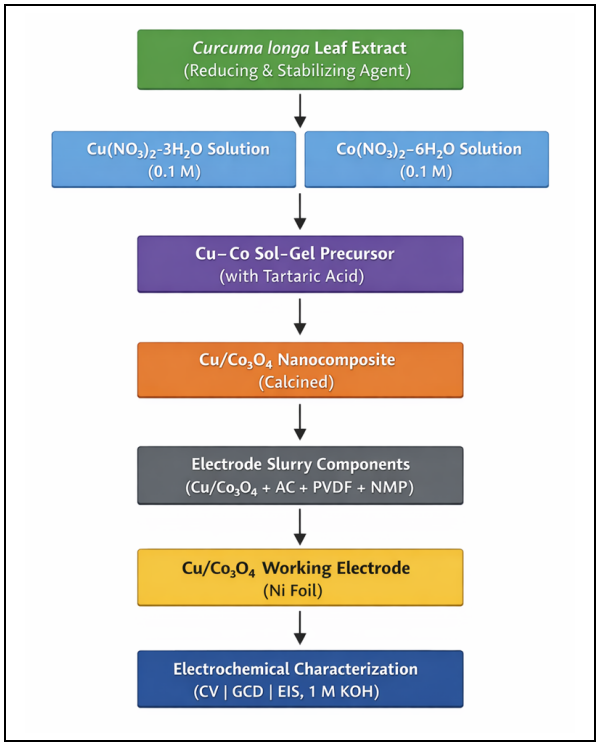


Fig. 1. Block diagram representing the green sol–gel synthesis of the Cu/Co_3O_4 nanocomposite

2.3 Characterization Techniques

This research employed UV-Vis spectrometer (UV 3600i Plus, Shimadzu) to analyze the optical properties of Cu/Co_3O_4. Fourier Transform Infrared spectrometer with resolution of ±4 cm^{-1} was used to conduct functional group analysis within the 4000 to 400 cm^{-1} range. A Powder X-ray diffractometer (Bruker D8 Advance) was employed for the structural examination. To analyze the structure, chemical composition, and distribution of these components, scanning electron microscopy (SEM with EDAX, ZEISS GEMINI) was employed to investigate the samples. TGA/DTA apparatus (Model: SDTQ600, USA) was employed to assess the thermal stability of the product.

2.4 Electrochemical Characterization Method

The electrochemical workstation was utilized to measure Cu/Co_3O_4. The reference electrode comprised of a platinum wire, current collector utilized Cu/CuCl, and the working electrode consisted of Cu/Co_3O_4. A three-electrode system was employed to analyze the performance of the working electrode, while a two-electrode method was utilized to assess the asymmetric supercapacitor. The electrolyte comprised 1 mole of a concentrated KOH solution.

2.5 Preparation of Working Electrode (Cu/Co_3O_4)

Working electrode was fabricated by 10% polyvinylidene fluoride (PVDF-binder), combining 80% activated carbon (AC) and 10% Cu/Co_3O_4 Nano powder in a mortar. The incorporation of *N*-methyl-2-pyrrolidone solvent transformed this mixture into a slurry. Subsequently, Dr. Blade technique was employed to apply a coating of the resulting slurry onto a nickel foil (1 × 1 cm^2), which was then allowed to dry overnight at 60 °C. The weighing scale indicated that 0.095 mg of active material with an approximate thickness of 5 µm was applied to the nickel foil.

3. RESULTS AND DISCUSSION

3.1 UV–Vis Evaluation

The optical characteristics of nanosized Cu/Co_3O_4 are illustrated in Fig. 2. The absorption edge was detected at 333.1 nm for Cu-implanted Co_3O_4 nanoparticles and at 373.3 nm for Cu/Co_3O_4. The absorption edge was shifted towards the visible spectrum and exhibited high sensitivity to solar light irradiation. Cu/Co_3O_4 can generate a large number of electron-hole pairs to destroy the dye. Previous research indicated that UV–Vis examination demonstrated significant absorption in the 400–700 nm range and a decreased optical band gap for CdO–CuO–ZnO–Co_3O_4 nanocomposite, signifying improved charge transport properties and higher visible-light absorption (Abdulwahab *et al*. 2025).

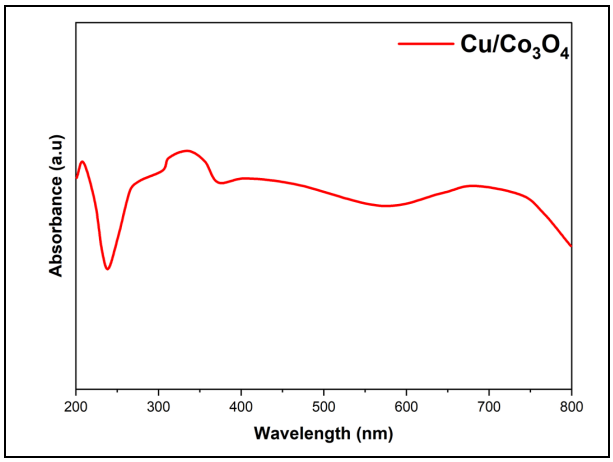


Fig. 2. Absorption spectrum of the synthesized Cu/Co_3O_4 nanocomposite

The following presents the outcome of determining the bandgap of the Cu/Co_3O_4 nanocomposite by Tauc's plot methodology.

$$h\nu\alpha = A\left(h\nu - E_g\right)^{1/2} \quad \ldots (1)$$

The constants h, v, α, and E_g show the absorption coefficient, frequency, Planck constant and bandgap, respectively. The optical band gap of the Cu/Co_3O_4 nanocomposite, estimated from the Tauc plot, is approximately 2.0 eV, indicating enhanced absorption in the visible region. A reduced band gap generally suggests improved electronic conductivity and charge-carrier mobility within the material. However, the influence of optical properties on electrochemical performance is indirect and should be considered in combination with other critical factors such as morphology, surface area, redox-active sites, and ion diffusion pathways. Therefore, the enhanced electrochemical behavior observed for the Cu/Co_3O_4 electrode cannot be solely attributed to band gap reduction. The reduction of the band gap indicative of enhanced conductivity, consequently, offers an indirect method to investigate the functionality of the supercapacitor. Accordingly, UV–Vis analysis primarily confirms favorable optical characteristics, while electrochemical performance is governed by a synergistic interplay of structural and interfacial properties.

3.2 TGA/DTA Evaluation

Degradation of Cu/Co_3O_4 occurs in four phases and are analyzed using TGA and DTA tests as depicted in Fig. 3. Within the temperature range of 30–200 °C, the initial phase is attributed to the elimination of adsorbed or trapped water with a mass loss quantified at 0.607%. During the temperature interval of 200–500 °C, the second step yields a loss of 0.810%. The third stage occurs within temperature of 500–900 °C, resulting in a maximum mass loss of 7.221%. The fourth stage of weight loss transpires within a temperature range of 900–1000 °C, corresponding to the minimal mass loss of 0.440%. The remnant of the final mass loss consists of Cu/ Co_3O_4 (90.92%). The TGA curve results were validated by DTA curves, which exhibited three endothermic peaks at 114.0, 326.7, 838.8, and 939.9 °C. Previous studies indicate that TGA analysis validated the thermal stability of the Co_3O_4/MoCo/LDH electrode, demonstrating gradual weight loss linked to moisture evaporation and LDH decomposition, hence affirming its appropriateness for high-temperature supercapacitor applications (Zarean *et al*. 2022).

3.3 FTIR Evaluation

The FT-IR spectrum the pure samples and Cu/ Co_3O_4 was obtained in the 400-4000 cm^{-1} region to identify chemical bonds and functional groups present at the materials (Fig. 4). The absorption peaks at 549 and 609 cm^{-1} correspond to Cu stretching vibrations of copper in the monoclinic system. The bands observed at 664-563 cm^{-1} are attributed to metal oxides in the nanocomposite. The stretching bands for the Td system in Co_3O_4 are observable at 669 cm^{-1} and 598 cm^{-1}, respectively. A prominent peak at 1690 cm^{-1} is indicative of the OH vibration of water molecules physically adsorbed on the surface of the nanocomposite. The stretching vibrations between 3077 and 3641 cm^{-1} correspond to the –OH groups of water molecules. The FT-IR spectrum offers significant insights into the chemical composition and functional groups contained in the produced materials. The FTIR spectrum of the synthesized particles derived from *Curcuma longa* leaf extract exhibited the distinctive peaks of MoO_3, ZnO, and g-C_3N_4, thus, validating the successful production of the composite. The minor peak changes suggest an interaction between the functional groups of the leaf extract and the photocatalyst surface, as documented in the literature (Gautam *et al*. 2023).

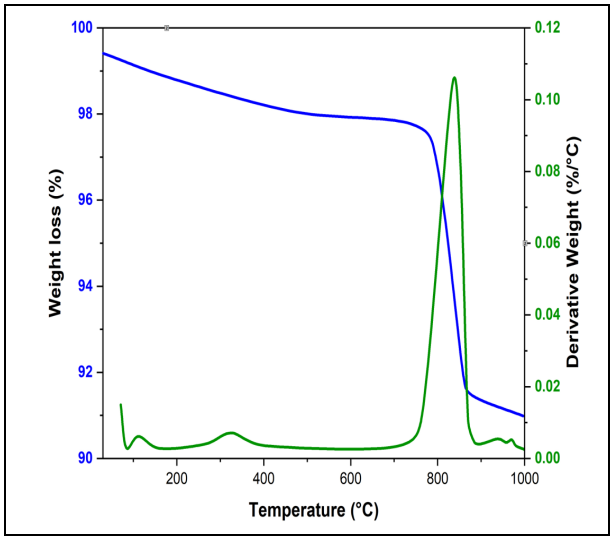


Fig. 3: TGA/DTA of Cu/Co_3O_4 nanocomposite

3.4 XRD Analysis

X-ray diffraction (XRD) studies were conducted to ascertain the crystalline phases of Cu/ Co_3O_4, as illustrated in Fig. 5. The XRD pattern of the synthesized Cu/Co_3O_4 nanocomposite exhibits characteristic diffraction peaks corresponding to the cubic spinel structure of Co_3O_4, consistent with JCPDS card No. 42-1467. The prominent reflections observed at 2θ values of approximately 31.3°, 36.8°, 44.8°, 59.3°, and 65.2° are indexed to the (220), (311), (400), (511), and (440) crystallographic planes, respectively. Minor peak shifts are attributed to Cu incorporation into the Co_3O_4 lattice, while the absence of secondary phases confirms successful composite formation. The full-width

at half maximum (FWHM) increased from 0.21° (undoped) to 0.26° (3% Cu) and 0.29° (6% Cu), indicating lattice deformation and defect formation (Sunil *et al*. 2024).

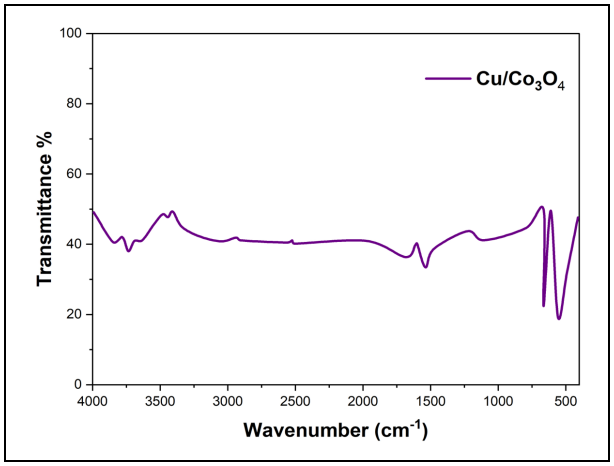


Fig. 4: Characteristic FTIR vibrational peaks of Cu/Co_3O_4

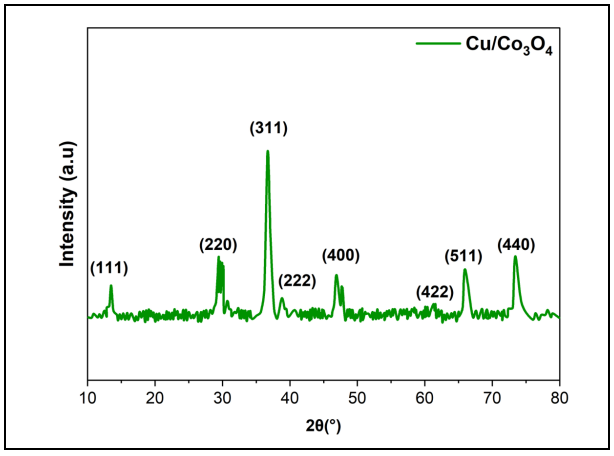


Fig. 5: XRD analysis validating crystalline phases in Cu/Co_3O_4

Subsequently, the Scherrer equation was employed to ascertain the crystallite size of the Cu/ Co_3O_4 nanocomposite derived from its corresponding XRD pattern.

$$D = \frac{K\lambda}{\beta \cos\theta} \quad \ldots (2)$$

The variables employed in this equation comprise crystallite dimension (D), FWHM (β), and the wavelength of Cu Kα radiation (λ) (1.5406 Å). The crystallite size obtained from the Scherrer equation (~35 nm) represents the coherent diffraction domain size and is considered the most realistic estimate for the synthesized Cu/Co_3O_4 nanocomposite. It was closely examined by Williamson-Hall formula (3).

$$\beta \cos\theta = 4\varepsilon \sin\theta + \frac{K\lambda}{D} \quad \ldots (3)$$

The crystallite size was 1.54 nm, while ε denotes strain. Fig. 6 indicates that the W-H plot produced an estimated crystallite size of 126 nm. Both values indicate actual size of Cu /Co_3O_4 nanocomposite grains. The crystallinity ratio was also calculated using equation (4).

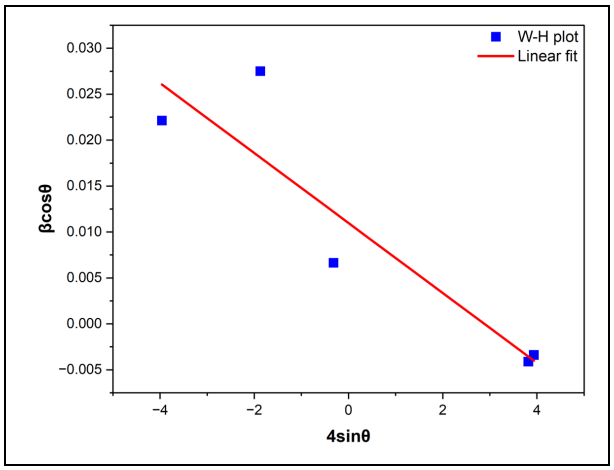


Fig. 6: W–H graph

$$\text{Crystallinity} = \frac{\text{Crystalline spike area}}{\text{area}} \times 100\% \quad \ldots (4)$$

The encapsulated organic substance exhibits a crystallinity of 82.75%. The apparent lower value derived from the Williamson–Hall intercept arises from strain-dominated peak broadening and does not reflect actual particle dimensions, while the larger size estimated from Rietveld refinement corresponds to agglomerated crystalline domains. Therefore, the Scherrer-derived value is reported as the representative crystallite size, with the other methods serving as complementary structural indicators.

Table 1. Structural variables of Cu/Co_3O_4

Parameters	GOF	a = b = c (A)	Phase content (%)	Density (e/Å^3)	Volume (Å^3)	R (obs) (%)
Organic molecule	-	-	1.1	-	-	
Cu	1.18	3.615	99.0	2.85	47.2	1.6
Mn_3O_4	1.18	8.084	98.2	4.02	527.8	1.84

3.5 SEM with EDAX

Fig. 7a illustrates the shape and elemental content of Cu/Co_3O_4 nanocomposite. The diameter was quantified as 96–127 nm utilizing ImageJ software. Nanorods were seen in clusters with agglomeration, which is attributed to strong interparticle interactions and residual organic species from the plant extract. While agglomeration may reduce the effective surface area and limit electrolyte accessibility to some active sites, it can also enhance electrical connectivity between particles, thereby facilitating charge transport during electrochemical cycling. Fig. 7b illustrates the elemental composition of the Cu/ Co_3O_4 nanocomposite. The elemental analysis reveals a predominant presence of oxygen (57.6wt%), accompanied by cobalt (30.8 wt%) and copper (11.6 wt%), thereby substantiating the establishment of a mixed metal oxide system. The encapsulation of bio-compounds was established, aligning with other confirmed chemical and physical properties of nanocomposites. Previous research indicated that SEM pictures revealed uniformly distributed nanostructures anchored to the GO surface, indicating their well-formed nature (Kandasamy *et al.* 2026). EDAX analysis confirms the presence of Cu, Co, and O as the major constituent elements of the nanocomposite, with oxygen as the dominant component followed by cobalt and copper; minor variations in weight percentage are attributed to the semi-quantitative nature of EDAX analysis and compositional heterogeneity.

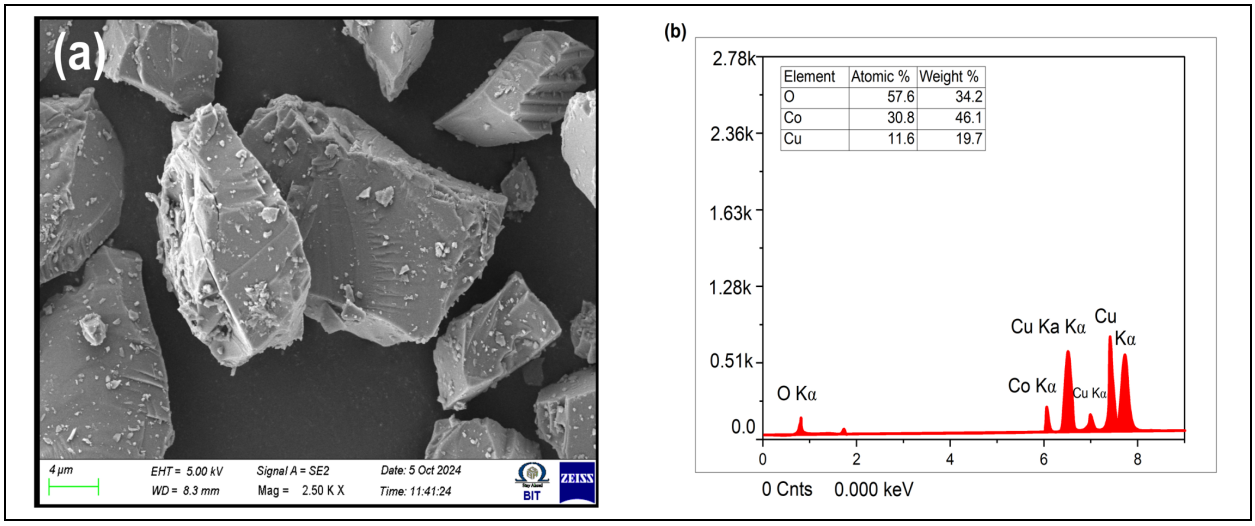


Fig. 7: SEM with EDAX evaluation of Cu/Co_3O_4 nanocomposite

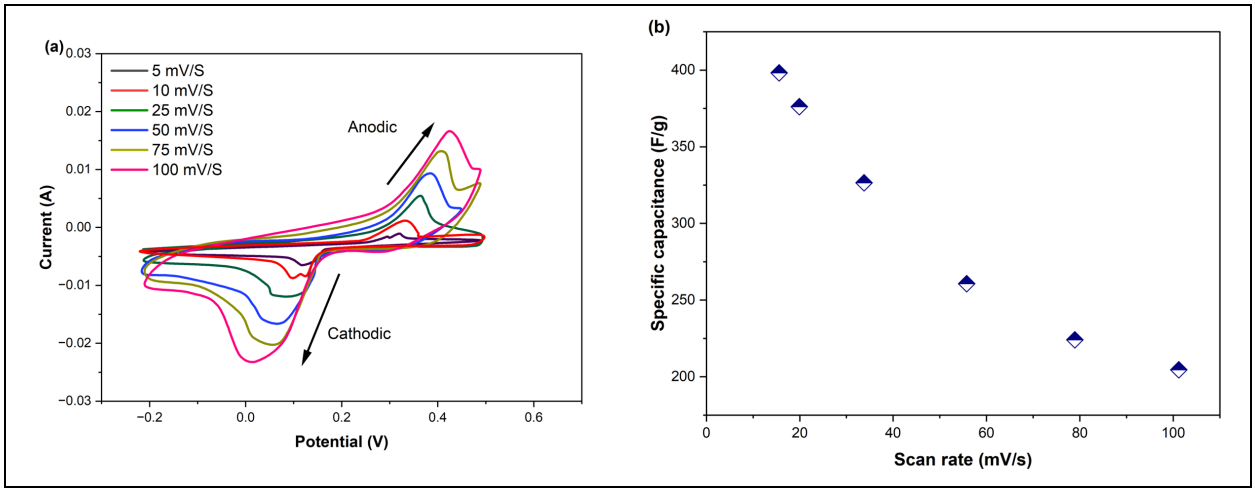


Fig. 8: CV analysis and capacitance variation with scan rates

3.6 Electrochemical Investigations

Electrochemical impedance spectroscopy, cyclic voltammetry and galvanometric analysis was used to study Cu/Co_3O_4 nanocomposite electrode properties.

3.6.1 Cyclic Voltammetry

Fig. 8a illustrates the outcomes of cyclic voltammetry for Cu/ Co_3O_4 within potential range of -0.2 - 0.4 V (Cu/CuCl). The Cu/Co_3O_4 nanocomposite has pseudocapacitive behavior, evidenced by the presence of anodic and cathodic peaks in its behavior curves during oxidation and reduction processes. The behavior depicted in Fig. 8b altered with variations at scan rate likely because of influence of both non-faradaic and faradaic processes at the electrode surfaces. Although the polarization of the active material (Cu/ Co_3O_4) resulted in the oxidation/reduction peaks shifting to higher and lower potentials, the electrode nevertheless demonstrates commendable reversibility. As noted in earlier research, cyclic voltammetry showed pronounced redox peaks and superior charge-storage behavior for both $Cu_xCo_{3-x}O_4$@Cu_2O and MOF-derived $CuCo_2O_4$ electrodes compared to pristine oxides. These enhanced CV responses confirm their strong electrochemical activity for high-performance energy-storage applications (Khered *et al*. 2025).

The following equation shows how oxidation/reduction peaks appear for Cu/ Co_3O_4.

$$xH^+ + xe^- + \frac{Cu}{Mn_3O_4} \leftrightarrow H_xCuMn_3O_4 \quad \ldots(5)$$

$$(Cu/Mn_3O_4)_{surface} + xH^+ + xe^- \leftrightarrow (Cu/Mn_3O_4 - H_x^+)_{surface} \ldots(6)$$

The relations used to compute specific capacitances with active integration area are,

$$C_{sp}(\text{ gravimetric }) = \frac{\int Idv}{mv\Delta V} \quad \ldots(7)$$

$$C_{sp}(\text{ Volumetric }) = C_{sp}\ (\text{gravimetric}) \times \rho \quad \ldots(8)$$

The variables I, m, Δv, ρ, and v represent the applied current, scan rates, mass of active material and potential window. At scan speeds of 5, 10, 25, 50, 75, and 100 mVs^{-1}, estimated gravimetric specific capacitances were 375, 325, 300, 235, 200, and 185 Fg^{-1}. Fig. 9(a) illustrates the correlation among calculated scan rates and specific capacitances. It was noted that the scan speeds raised from 5 to 100 mV s^{-1}, there was a reduction. The rise in specific capacitances is attributed to the valence state of Mn ions, which enhances ionic conductivity and facilitates accelerated ion transit across electrode surfaces. Cu/ Co_3O_4 has pseudocapacitive charge storage behavior characterized by Faradaic processes, governed by (i) diffusion control and (ii) capacitive mechanisms. The operation of this integrated charge storage system on current's response to applied sweep rates. Thus, the subsequent equation was employed to estimate the kinetic limitations.

$$i(V) = aV^2 \quad \ldots(9)$$

The parameters a and b are adjustable, and I acquired the current at the sweep rate. A value of 1 for b indicates capacitive control, whereas a value of 0.5 signifies diffusion control. This is an analysis of the two elements comprising this combination.

$$i(V) = k_1v + k_2v^{\frac{1}{2}} \quad \ldots(10)$$

$$\frac{i(V)}{v^{0.5}} = k_1v + k_2 \quad \ldots(11)$$

Here, k_1v and k_2v represent the cumulative effects of applied potentials governed by diffusion and surface control, respectively. Equation (6) produces the b-value of approximately 0.44 indicating that the charge-storage process is predominantly diffusion-controlled, with a minor contribution from surface capacitive effects. Cu/ Co_3O_4 indicates that the electrode exhibits Faradaic behavior due to the ions distributed on electrolyte / electrode interface. The diffusion process is the only recognized mechanism for battery-type Faradaic reactions. The linear relationship between the cathodic and anodic currents and their scan produces the intended outcome, as depicted in Fig. 9(b). Fig. 10(a) illustrates the fitted values of I (V) v0.5, enabling the quantification of charge storage contributions as per equation (6). Fig. 10(b) illustrates diffusion-controlled predominance. Fig. 10(c) illustrates the experimental results at scan rate of 25 mV/s, demonstrating that Cu/ Co_3O_4 electrode exhibits more significant diffusion-controlled storage mechanism. However, due to its surface control, it also exhibits capacitive properties. In charge-discharge analysis, non-linear chronopotentiometry curves represent the obtained data corroborated by extensive charge transfer peaks.

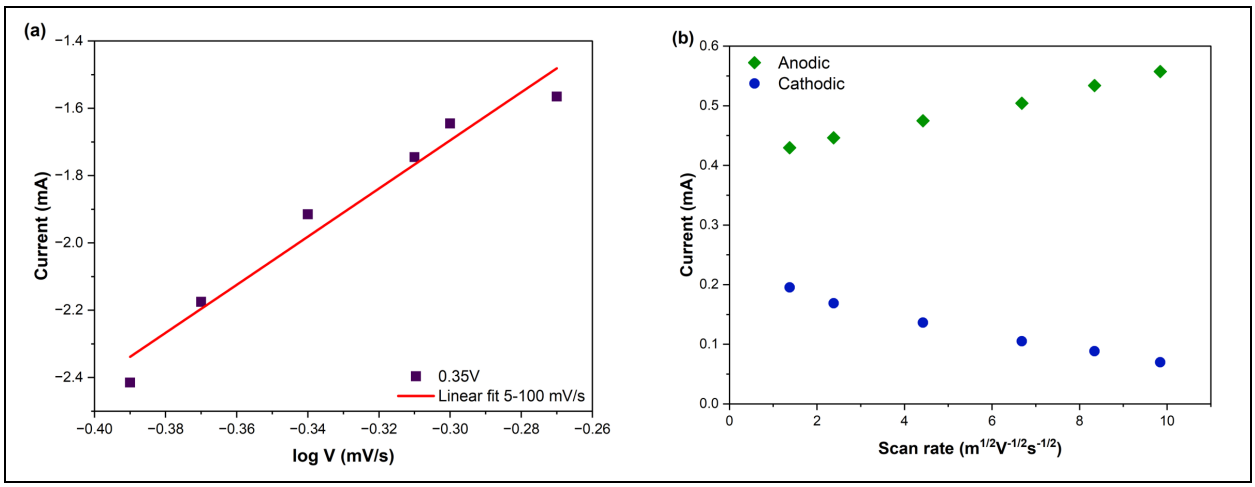


Fig. 9: Linear relation and b-value

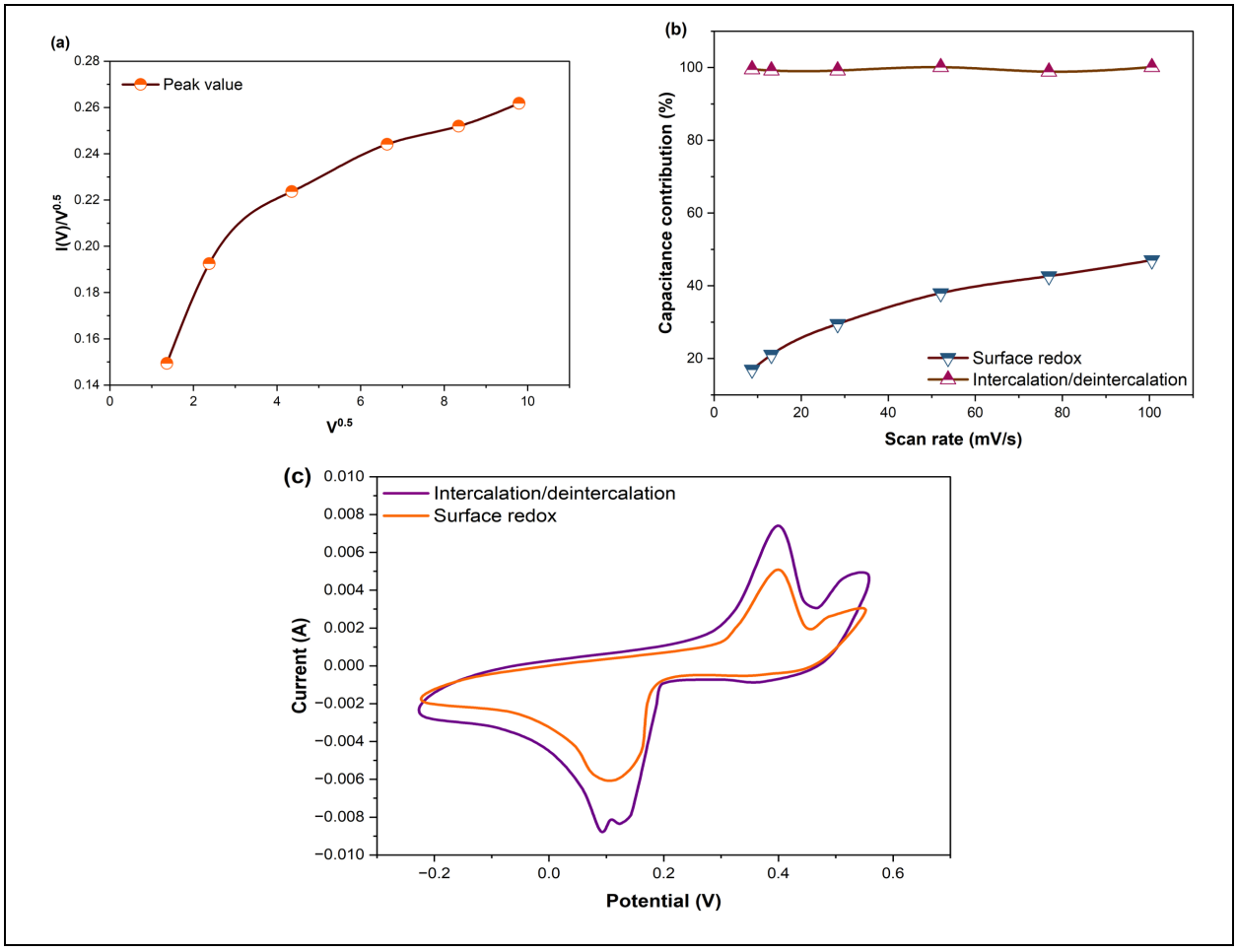


Fig. 10: Capacitance contributions at various electrochemical scan rates

3.6.2 Galvanometric Profiles

Fig. 11(a) illustrates the charge-discharge characteristics of the Cu/ Co_3O_4 electrode. The experimental current density ranged from 1 to 5 mAg^{-1}, whereas the potential range was 0 to 0.6 V.

The profiles elucidate the results of CV curves and exhibit non-linear curves marked by asymmetrical electrode action. As reported in previous research, the GCD curves displayed an asymmetric triangular shape, confirming good capacitive behavior and stable charge–discharge reversibility. This characteristic indicates

efficient energy storage capability of the ZC/Cu electrode (Aljawrneh *et al*. 2025). To ascertain specific capacitance of electrode, discharge duration from GCD curves and the mathematical relationship presented below was used.

$$c_{sp} = \frac{I\Delta t}{\Delta V m} F g^{-1} \quad \ldots (12)$$

The potential window, ΔV, discharge duration, and applied current, I are all variables. The specific capacitances for third, first, and second orders were 345, 315, 196, 147 and 128 Fg^{-1}, respectively. Current density of 1 A/g and the specific capacitance measured 345 Fg^{-1} indicate notably high value. The obtained specific capacitance of 345 F g^{-1} at 1 A g^{-1} is comparable to or higher than many reported Cu–Co oxide-based electrodes synthesized *via* conventional routes, demonstrating the effectiveness of the present green synthesis approach. Fig. 11(b) illustrates that when the applied current density increases, the calculated specific capacitance correspondingly diminishes. Decreased specific capacitances at elevated scan speeds may result from limited availability of OH− ions among the electrolyte interface and electrode. Electrochemical impedance spectroscopy was employed to evaluate the kinetics of charge transfer at interfaces due to its significance in the charge storage system. An applied current of 3 mA/g was utilized to evaluate the cyclic stability of the fabricated electrode. Fig. 11c indicates that following 5000 cycles, the cyclic retention was 95.3%, and the projected coulombic efficiency attained 99%. Although the Cu/Co_3O_4 electrode exhibits excellent capacitance retention over 5000 cycles, extended cycling beyond this range would be required to fully establish long-term durability, which is proposed as part of future investigations. These findings make the fabricated electrode a viable candidate for future real-time energy storage applications.

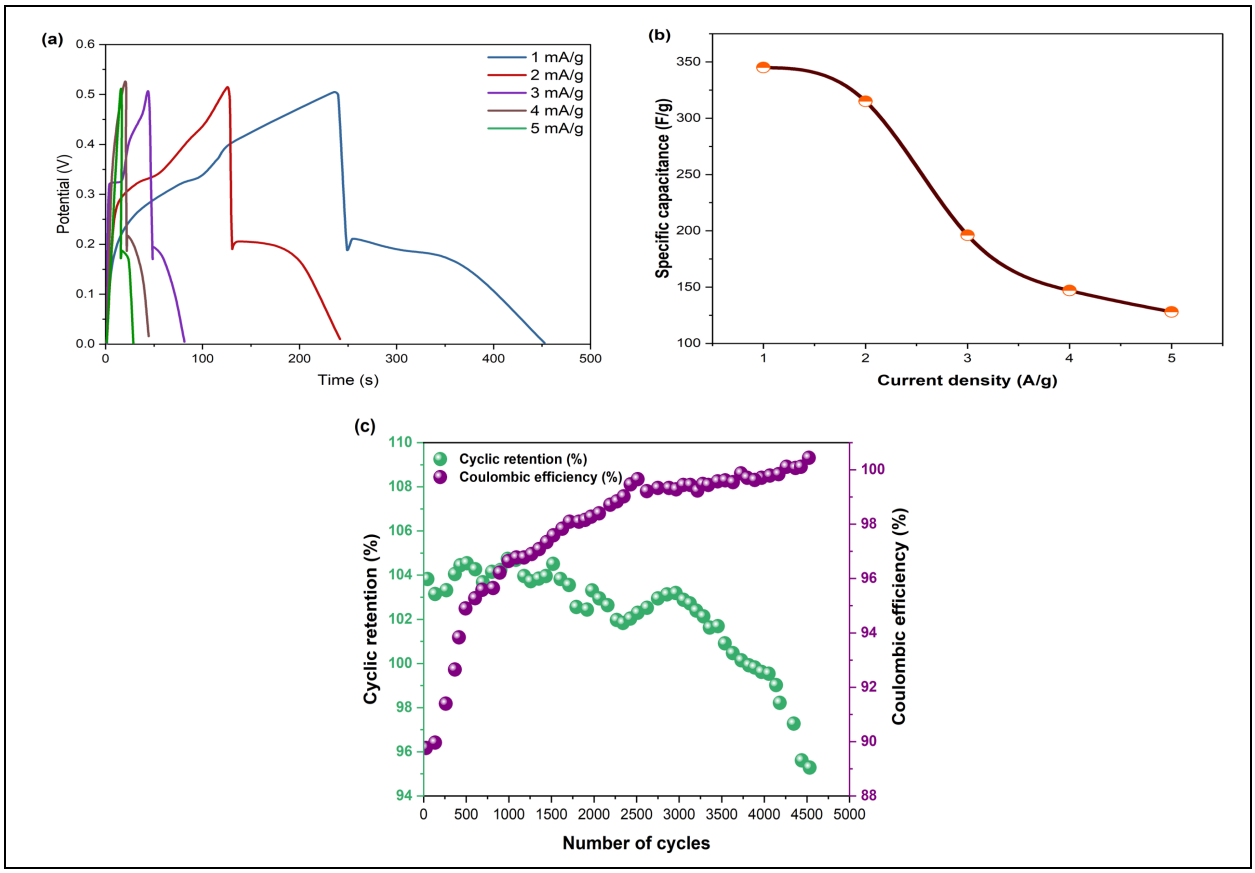


Fig. 11: GCD analysis of Specific capacitance versus current density for Cu/Co_3O_4

3.6.3 EIS Analysis

Fig. 12 illustrates the EIS spectrum of Cu Co_3O_4, elucidating the charge storage kinetics. At elevated frequencies, the Cu/ Co_3O_4 electrochemical impedance spectroscopy (EIS) or Nyquist plot exhibits a semicircular arc; at diminished frequencies, it presents a linear trajectory. Z-view was employed to simulate the EIS spectrum. The equivalent circuit used for fitting the EIS data consists of the solution resistance (R_s), charge-transfer resistance (Rct), constant phase element (CPE), and Warburg impedance (W), representing ion diffusion

at low frequencies. The fitted parameters are summarized in Table 2, where each element corresponds to a distinct electrochemical process at the electrode–electrolyte interface. At low frequencies, semicircle represents combined constant phase element and charge transfer resistance. The values of Rct were found to be 0.96 Ω before GCD analysis and 0.61 Ω after it. To enhance charge storage at the electrode, one should target a low Rct value following GCD analysis. This will facilitate increased electron and ion transit at the electrode/electrolyte interface, enhancing energy storage capabilities. The Warburg impedance observed in the low-frequency region reflects the diffusion-controlled transport of electrolyte ions within the Cu/Co_3O_4 electrode. The inclined line in the Nyquist plot indicates efficient ion diffusion, which contributes to the pseudocapacitive charge-storage behavior of the electrode. This demonstrates that the CO3- and transition metal intercalation electrode serves as the locus of the redox process. The findings of the Cu Co_3O_4 electrode are corroborated by variations observed at the GCD and the features of Nyquist plot, which exhibits an angle of around 45°. This study demonstrates exceptional electrochemical efficiency for specific capacitance with a little quantity of electrolyte solution. Moreover, it offers significant environmental advantages and has exceptional durability. Previous work demonstrated that the EIS analysis confirmed low charge-transfer resistance for the Co_3O_4/PAN CNF electrodes, indicating efficient ion diffusion and fast interfacial kinetics. The improved impedance response validates their strong suitability for high-performance supercapacitor applications (Mohite *et al*. 2024).

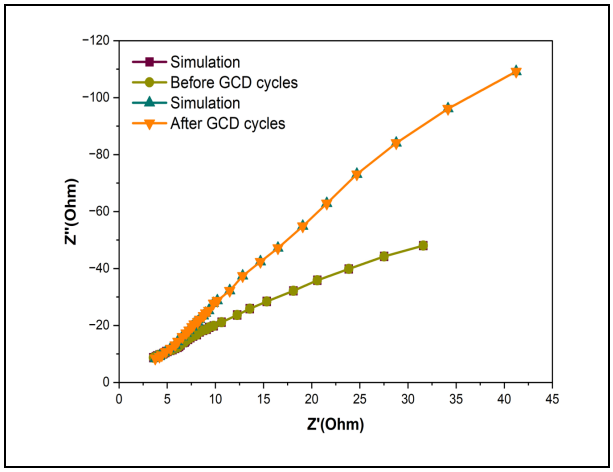


Fig. 12: EIS response of Cu/Co_3O_4 electrode and circuit

Table 2. EIS-derived fitted parameters for Cu/Co_3O_4 electrode

Charge Transfer Resistance (R_{ct})	Solution Resistance Ohm (R_s)	Warburg Impedance (W)	Constant Phase Element (CPE)
0.22	3.11	1.22	0.14

4. CONCLUSIONS

A Cu/Co_3O_4 nanocomposite was successfully synthesized *via* a green sol–gel method using *Curcuma longa* leaf extract as a natural reducing and stabilizing agent. Structural and morphological analyses confirmed the formation of a spinel Cu/Co_3O_4 nanocomposite with nanorod-like features, while FTIR and XRD results verified phase purity and successful composite formation. Electrochemical investigations demonstrated dominant Faradaic pseudocapacitive behavior, delivering a specific capacitance of 345 F g^{-1} at 1 A g^{-1} with 95.3% capacitance retention after 5000 cycles and low charge-transfer resistance, indicating efficient charge transport. Although the electrode exhibits diffusion-controlled charge storage with promising stability, extended cycling and device-level studies are required to further assess long-term durability and practical applicability. The results highlight the potential of green-synthesized Cu/Co_3O_4 nanocomposites as effective electrode materials for supercapacitor applications.

FUNDING

This research received no specific grant from any funding agency in the public, commercial, or not-for-profit sectors.

CONFLICTS OF INTEREST

The authors declare that there is no conflict of interest.

COPYRIGHT

This article is an open-access article distributed under the terms and conditions of the Creative Commons Attribution (CC BY) license (http://creativecommons.org/licenses/by/4.0/).

REFERENCE

Abdulwahab, A. M., Aldeen, T. S. and Aziz, S. N., Synthesis and characterization of multifunctional CdO–CuO–ZnO–Co_3O_4 nanocomposite, *Res. Phys*., 75, 108335 (2025). https://doi.org/10.1016/j.rinp.2025.108335

Alaş Çolak, M. Ö., Passos, A. L., Güngör, A., Erdem, E. and Genç, R., Nanoarchitectonics of polyaniline derived carbon electrodes incorporating transition metal oxides for supercapacitor devices, *J. Power Sources,* 645, 237230 (2025). https://doi.org/10.1016/j.jpowsour.2025.237230

Aljawrneh, B., Albiss, B. A., Amani, A., Muhammad, T., Abdelelah, A., Saja, A. and Rawan, H., Ultrathin zinc cobalt oxide nanowalls for supercapacitive energy storage applications, *Energy Nexus*, 18, 100439 (2025). https://doi.org/10.1016/j.nexus.2025.100439

Anantha, R. L., Satishkumar, P., Nagabhooshanam, N., Rao, P. K. V., Kumar, D. S., Antharaju, K. C., Prasad, Y. D. and Mohanavel, V., Shear strength, wear, thermal conductivity, and hydrophobicity behavior of fox millet husk biosilica and Amaranthus dubius stem fiber–reinforced epoxy composite: a concept of biomass conversion, *Biomass Convers. Biorefin*., 15(2), 2893–2901 (2025). https://doi.org/10.1007/s13399-023-04854-x

Anekwe, I. I., Chikwendu, C. I., Amadi, E. S., Nwogwugwu, N. U. and Ihenetu, F. C., Gas chromatography–mass spectrometry analysis of bioactive compounds of *Curcuma longa* leaves extract, *Int. J. Biol. Chem. Sci*., 17(3), 1199–1207 (2023). https://doi.org/10.4314/ijbcs.v17i3.34

Da Silva, H. J., Rafael, R. A., Allan, J. M. A., Oliveira, D. A. L. M., Daniel, M. A., Lemos, S. G. and Silva, D. F. F., Bifunctional MOF-on-MOF-derived $CuCo_2O_4$ for oxygen evolution reaction electrocatalysis and supercapacitor electrodes, *ChemistryOpen*, (2025). https://doi.org/10.1002/open.202500180

Din, U. M. M., Batool, A., Ashraf, R. S., Yaqub, A., Rashid, A. and Din, N. U. M., Green synthesis and characterization of biologically synthesized and antibiotic-conjugated silver nanoparticles followed by post-synthesis assessment for antibacterial and antioxidant applications, *ACS Omega,* 9(17), 18909–18921 (2024). https://doi.org/10.1021/acsomega.3c08927

Ganvir, H. V., Kumar, S., Kumar, R., Hadar, B., Satishkumar, P., Ravi, V., Dolas, D. R., Arun, V., Jadhav, V. D. and Selvaraju, M., Monitoring atomic layer deposition by potentiodynamic electrochemical impedance spectroscopy of multielement adlayers, *J. New Mater. Electrochem. Syst.*, 27(3), 172–181 (2024). https://doi.org/10.14447/jnmes.v27i3.a02

Gautam, N., Singh, K. B., Deen, D. U., Sanjay, S. and Pandey, G., Fabrication of *Curcuma longa* mediated Ni@ZnO/MoO_3 composite anchored with g-C_3N_4 for sunlight driven photocatalytic activity, *Opt. Mater*., 142, 114041 (2023). https://doi.org/10.1016/j.optmat.2023.114041

González-Banciella, A., Artigas-Arnaudas, J., Martinez-Diaz, D., Sanchez, M. and Ureña, A., Carbon fiber-based asymmetric supercapacitors with MOF-derived Cu-doped Fe_2O_3 and Ni-doped Co_3O_4 coatings, *Compos. Part A Appl. Sci. Manuf*., 200, 109292 (2026). https://doi.org/10.1016/j.compositesa.2025.109292

Gopan, G. S. S., Nelsa, A., Rani, S., Dona, K. and Alana, K. M., *Curcuma longa* derived heteroatom self-doped porous carbon for cost-effective solid-state supercapacitors, *Chem. Nano. Mat.,* 11(1), (2025). https://doi.org/10.1002/cnma.202400505

Gopinath, S., Mayakannan, M. and Vetrivel, S., Structural, optical and morphological properties of silver doped cobalt oxide nanoparticles, Ceram. Int., 48(5), 6103–6115 (2022). https://doi.org/10.1016/j.ceramint.2021.11.149

Hari, K. B., Parthasaradhi, R. C., Reddy, P. P., Mallikarjuna, K., Reddy, N. I. and Bai, C., Copper cobalt oxide microstructures resembling marigold flowers synthesized by solvothermal method for high-performance supercapacitors, *Inorg. Chem. Commun.,* 160, 111922 (2024). https://doi.org/10.1016/j.inoche.2023.111922

Kandasamy, N., Shanmugam, P., Lalitha, G., Mani, A., Gowsalya, V., Subbramaniyan, P. and Venugopal, T., Facile synthesis of graphene oxide supported metal doped cobalt oxide nanostructures as an active electrode material for supercapacitor applications, *Mater. Chem. Phys*., 347, 131488 (2026). https://doi.org/10.1016/j.matchemphys.2025.131488

Khawale, V. R., Mayank, Ravi, K., Satishkumar, P., Barun, H., Deepa, B., Rajasekaran, S., Veeramanikandan, P., Babu, P. A. S. and Mayakannan, S., Study on electrochemical stability and charge transfer efficiency for the development of high-performance supercapacitors using iron oxide (Fe_2O_3) nanorods, *J. New Mater. Electrochem. Syst*., 27(3), 163–171 (2024). https://doi.org/10.14447/jnmes.v27i3.a01

Khered, M., Alsayigh, A. N., Raja, A. L., Naif, A. S., Nasser, A. and Aladeem, A. A., Enhanced synergistic redox behaviour of solution-processed mixed metal oxide composite for high-performance hybrid supercapacitors, *J. Sol-Gel Sci. Technol*., 116(3), 3077-3089(2025). https://doi.org/10.1007/s10971-025-07002-1

Kumar, A., Satpathy, B. K., Goyal, P., Rajnikant, U., Kiapi, M. R. A., Jasuja, K., Dhruv, M. and Superb, M. K., Bimetallic MOF-derived CuO–Co_3O_4 heterostructures as high-capacity electrodes for asymmetric supercapacitors, *Chem. Eng. J.,* 520, 165685 (2025). https://doi.org/10.1016/j.cej.2025.165685

Liu, Z., Cheng, L., Jia, Z., Xin, H., Shiyun, Z., Yuan, S., Bo, Q., Biao, Z. and Yi, J., Synthesis, characterization and catalytic performance of nanocrystalline Co_3O_4 towards propane combustion, *J. Solid State Chem*., 292, 121712 (2020). https://doi.org/10.1016/j.jssc.2020.121712

Mayakannan, M., Prabakar, S. and Vinoth, E., Synthesis and characterization of zinc-doped cobalt oxide nanoparticles and their antibacterial and antifungal activities, *Inorg. Nano-Met. Chem*., 53(12), 1329–1335 (2023a). https://doi.org/10.1080/24701556.2021.1992431

Mayakannan, M., Prabakar, S. and Vinoth, E., Synthesis of copper sulfate supported cobalt oxide nanoparticles through microwave irradiation assisted method, *Inorg. Nano-Met. Chem.,* 53(8), 831–836 (2023b). https://doi.org/10.1080/24701556.2021.1977820

Mendhe, A. C., Kore, A., Dhas, S. D., Aqsa, G., Kim, G., Pragati, T. N. and Kim, D., Crystal-tuned spinel copper cobaltite with vertically aligned nanoribbons for high-performance asymmetric coin cells, *Adv. Funct. Mater*., 35(38), 2501674(2025). https://doi.org/10.1002/adfm.202501674

Mohite, D. D., Sachin, S. C., Lokhande, P. E., Sumit, D., Vishal, K., Jagtap, C., Rednam, U., Salve, M., Chaure, N. B., Ali, A. B. and Kumar, Y. A., Electrochemical characterization of electrospun Co_3O_4/PAN-based carbon nanofiber composites for supercapacitor applications, *J. Mater. Sci.,* 59(25), 11440–11453 (2024). https://doi.org/10.1007/s10853-024-09852-6

Samatha, K. and Sagar, R., Pseudocapacitive behavior of (Fe, Cu)-based Co_3O_4 as high-performance electrode materials for solid-state stiff and flexible supercapacitors, *Energy Technol.,* 13(11), 2500271(2025). https://doi.org/10.1002/ente.202500271

Shuaib, U., Tousif, H., Riaz, A., Mubarik, F. E., Sajjad, A. and Imran, S., Chemically synthesized cobalt oxide incorporated copper hexacyanoferrate composite as an efficient supercapacitor electrode material, *J. Appl. Electrochem*., 54(2), 245–256 (2024). https://doi.org/10.1007/s10800-023-01957-1

Singh, S. R., Akshatha, S. J., Megha, A. B., Padti, A. C., Bhavi, S. M., Rao, K. S., Bothe, T., Bepari, A., Babu, R. Y. and Srinath, B. S., Eco-synthesized silver nanoparticles from *Curcuma longa* leaves: phytochemical and biomedical applications, *Next Nanotechnol*., 8, 100249 (2025). https://doi.org/10.1016/j.nxnano.2025.100249

Sunil, K. K., Reddy, L., Mohammad, R. H., Nipa, R., Jong, S. K. and Sang, W. J., Comprehensive characterization of octahedral Co_3O_4 doped with Cu inducing oxygen vacancies as a battery-type redox active electrode material for supercapacitors, *Ceram. Int*., 50(19), 34726–34739 (2024). https://doi.org/10.1016/j.ceramint.2024.06.280

Yesuraj, J., Senthamaraikannan, T. G., Lim, D.-H. and Kim, K., Construction of ternary $Zn_{0.5}Cu_{0.5}Co_2O_4$ spinel structure on nickel foam for high-energy-density asymmetric supercapacitors, *Small,* 21(10), 2407608(2025). https://doi.org/10.1002/smll.202407608

Zarean, M. K., Ensafi, A. A. and Rezaei, B., Co_3O_4/MoCo/layered double hydroxide nanosheets for asymmetric supercapacitors, ACS Appl. Nano Mater., 5(6), 8097–8104 (2022). https://doi.org/10.1021/acsanm.2c01236

Zhang, H., Wang, J., Chen, Q., Yao, L., Wang, M., Dong, J. and Qi, J., Oxygen vacancies-modulated Cu-substituted Co_3O_4 nanoarrays as an efficient battery-type electrode for hybrid supercapacitors, *J. Alloys Compd.,* 1039, 183055 (2025). https://doi.org/10.1016/j.jallcom.2025.183055